Low temperature co-evaporation of hollow γ–$CsPbI_3$ perovskite layers for solar cells

Pascal Becker[1,2], José A. Márquez[1], Justus Just[1,3], Amran Al-Ashouri[4], Charles Hages[1], Hannes Hempel[1], Marko Jošt[4], Steve Albrecht[4], Ronald Frahm[2] and Thomas Unold[1]

[1]Helmholtz-Zentrum-Berlin, Hahn-Meitner-Platz 1, 14109 Berlin, Germany

[2]Bergische Universitaet Wuppertal, Gausstrasse 20, 42119 Wuppertal, Germany

[3]Lund University, Paradisgatan 2, 22100 Lund, Sweden

[4]Young Investigator Group Perovskite Tandem Solar Cells, Helmholtz-Zentrum-Berlin, Hahn Meitner-Platz 1, 14109 Berlin, Germany

E-mail: unold@helmholtz-berlin.de

Abstract

The structure stability and optoelectronic properties of co-evaporated $CsPbI_3$ thin films with a wide range of [CsI]/[PbI_2] compositional ratios are investigated. We find that for CsI-rich growth conditions, $CsPbI_3$ can be synthesized directly at low temperature into the distorted perovskite γ– $CsPbI_3$ phase with Schottky-type defects and without detectable secondary phases. In contrast, PbI_2-rich growth conditions are found to lead to the non-perovskite δ-phase. Photoluminescence spectroscopy and optical pump-THz probe measurements show carrier lifetimes larger than 75 ns and charge carrier (sum) mobilities larger 60 cm^2/Vs for the γ-phase, indicating their suitability for high efficiency solar cells. Building on these results p-i-n type solar cells with a maximum efficiency exceeding 12 % and high shelf stability of more than 1200 h are demonstrated.

After the steep rise of hybrid organic-inorganic perovskite solar cells (PSCs) with certified power conversion efficiencies over 22 %,[1,2] fully inorganic PSCs with cesium replacing the organic anion have lately drawn significant attention due to their better thermal stability.[3,4] In particular, lead-based $CsPbX_3$ (X = I, Br) represents a promising candidate for high efficiency stable photovoltaic devices. While the band gap of $CsPbBr_3$ is about 2.3 eV,[5,6] and therefore too large for photovoltaic applications,[3] the band gap of $CsPbI_3$ of 1.76 eV is ideal for top cells in tandem applications in conjunction with low band gap bottom cells.[7] Solution processed thin films based on $CsPbI_3$ absorber layers recently have reached an efficiency of 15.7 %,[8] while the current world record for quantum dot solar cells was reported employing $CsPbI_3$ nanocrystals with efficiencies exceeding 13 %.[9]

Unfortunately, for $CsPbI_3$ thin films at room temperature the orthorhombic δ-phase with a band gap of 2.8 eV is thermodynamically favored over the desirable cubic perovskite α- and distorted perovskite tetragonal-β and orthorhombic-γ phases.[10,11] Thus at room temperature the material has the tendency to either form directly in the δ-phase or to undergo a spontaneous phase change into the δ-phase, making it difficult to obtain or retain $CsPbI_3$ films in the perovskite phase.[10] The identification of the room-temperature phase has been a matter of considerable debate, with a number of earlier literature reports suggesting the (metastable) presence of the cubic-α phase [12–14]. However, more recent reports demonstrated that the α-phase is only stable at high temperatures above 310 °C[10,15] and undergoes a phase transition into the β- and γ-phases when the samples are cooled down to ambient temperatures. In order to add clarity to this issue, special attention will be placed on the characterization of the crystal structure that $CsPbI_3$ adopts in this work. In order to obtain $CsPbI_3$ in the perovskite phase thin films are usually heated above 320 °C to convert the yellow δ-phase into the perovskite phase.[14,16–18] However, such high temperatures can damage organic charge transport layers or flexible substrates, which limits the application in p-i-n solar cell architectures and in tandem devices. Different approaches have been used to form and stabilize the perovskite phase of $CsPbI_3$ at lower temperature, for example the use of mixed halide perovskites with partial substitution of iodine by bromide ($CsPbI_{3-x}Br_x$),[19,20] or the [21,22] introduction of bismuth,[12] strontium,[23] sulfobetaine zwitterions[24], hydroiodic acid,[25,26] and of phenethylamine (PEA).[26–28]

In this work we show a direct route to synthesize $CsPbI_3$ in the distorted perovskite γ-phase by co-evaporation of CsI and PbI_2 at a substrate temperature of 50 °C without the need for a post-deposition annealing treatment. Our process results in thin films with a lateral gradient in composition which allows us to study in depth the composition-dependent structural and optoelectronic properties of this material system. To this end, contactless high throughput

characterization including time-resolved and calibrated absolute photoluminescence (PL) and optical pump THz probe (OPTP) spectroscopy is employed. Finally p-i-n-type solar cells were fabricated using the low temperature-deposited $CsPbI_3$ thus demonstrating the applicability of the deposition route presented here for devices manufacturing.

Structure, composition and chemical stability of the γ-$CsPbI_3$ phase. To evaluate the influence of the compositional deviations from stoichiometry of $CsPbI_3$ on the materials properties, thin-films were deposited by co-evaporation of CsI and PbI_2 on quartz glass at a substrate temperature of 50 °C as shown in ***Figure 1a*** (see methods in the SI).

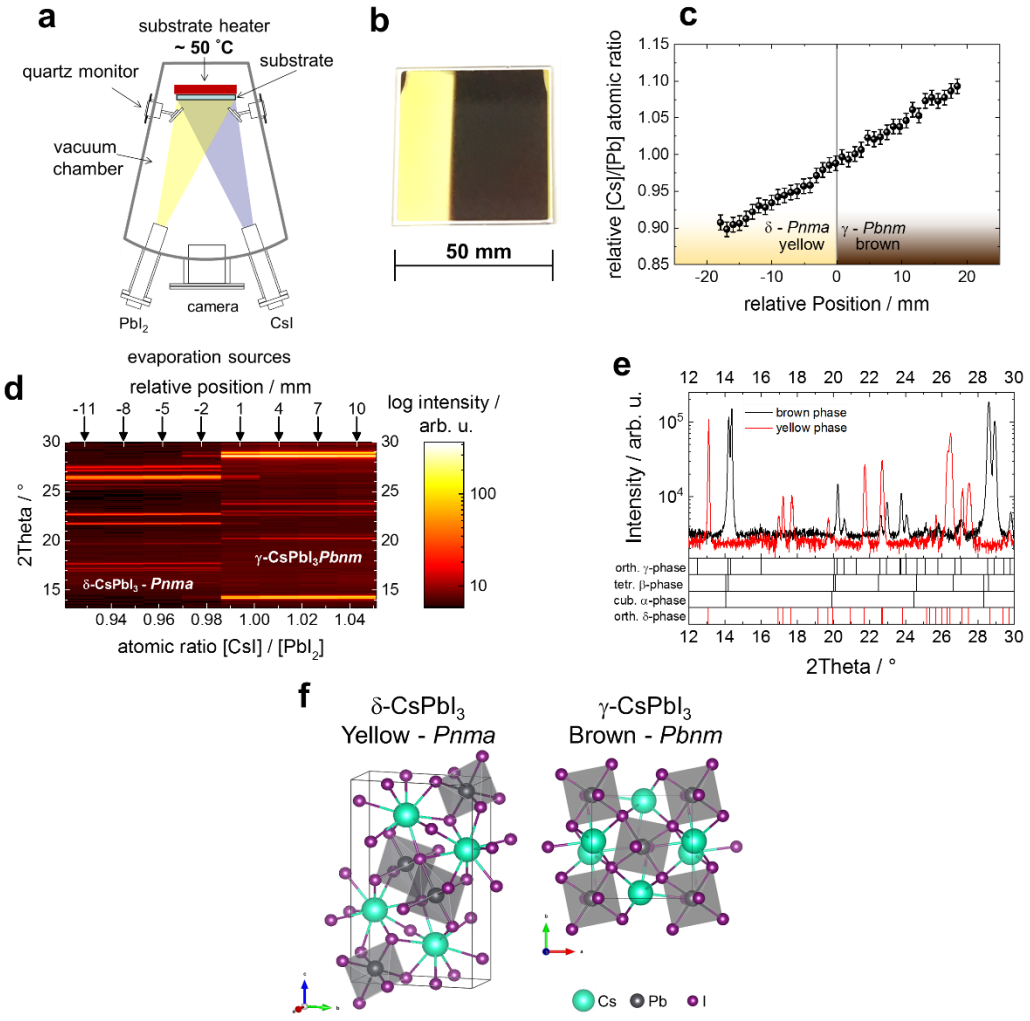

Figure 1 (a) *Schematics of the evaporation chamber used in this work.* ***(b)*** *Photographic image of an as-evaporated $CsPbI_3$ film. Two clearly distinct regions can be observed; one yellow, one brown.* ***(c)*** *[Cs]/[Pb] atomic ratio from XRF measurement as a function of position measured perpendicular to the phase boundary. The yellow and brown phases are color-labelled in the background* ***(d)*** *XRD patterns from a line scan for the combinatorial sample showing the phase transition as a function of composition (sample position). The arrows mark the positions at which measurements are taken.* ***(e)*** *XRD patterns*

acquired in the brown and yellow regions of the sample. ***(f)*** *Unit cells of the δ-$CsPbI_3$ (yellow – Pnma) and the γ-$CsPbI_3$ (brown – Pbnm) phases.*

The substrate is not rotated during deposition to allow the formation of a compositional gradient across the sample and the evaporation rates of both sources were controlled individually with quartz balance monitors. ***Figure 1b*** shows a photographic image of the as-evaporated sample where two clearly distinct regions can be observed, indicating the presence of a brown and a yellow phase with a distinct phase boundary. The chemical composition of the sample was analyzed by X-ray fluorescence (XRF) mapping. Error! Reference source not found.***c*** shows a line-scan perpendicular to the yellow-to-brown phase boundary. A monotonic, almost linear increase of the relative [Cs]/[Pb]-atomic ratio is observed moving from the yellow to the brown region of the sample, with a variation of the [Cs]/[Pb]-atomic ratio of more than 20 % across the 50 mm wide substrate. Interestingly, a stoichiometric 1:1:3 composition is observed directly at the phase boundary between the yellow and brown phase, although we note that the absolute uncertainty in the [Cs]/[Pb]-atomic ratio is estimated to be about 10 %.

To identify the structural properties of the sample as a function of composition an X-ray diffraction (XRD) line-scan was performed in direction of the chemical gradient. Error! Reference source not found.***d*** shows XRD patterns acquired as a function of sample position relative to the boundary between the two regions. Again a sharp boundary with distinctly different XRD patterns is observed between the yellow and brown regions of the sample within the experimental resolution. Typical diffractograms for the yellow and brown phase, respectively, are shown in Error! Reference source not found.***e***. Comparison with reference peak positions shows that the observed phases can only be assigned to the distorted perovskite γ-$CsPbI_3$ (space group *Pbnm*) in the brown region and the non-perovskite phase δ-$CsPbI_3$ (space group *Pnma*) in the yellow region.[10] This confirms that the stable perovskite at room temperature is the γ–$CsPbI_3$ and not the cubic α phase, in agreement with some recent studies.[10,15,29,30] Le Bail analysis was performed for the patterns acquired in the laboratory for both phases taking as starting models the δ and γ phases reported by Marronnier et al.[10] The analysis resulted in the δ-phase with lattice parameters a = 10.471 ± 0.002 Å, b = 4.790 ± 0.001 Å and c = 17.781 ± 0.003 Å, and the γ-phase with a = 8.629 ± 0.001 Å, b = 8.834 ± 0.001Å and c = 12.472 ± 0.002 Å (see ***Figure S1*** and ***Table S1***). We note that the lattice parameters values obtained for the γ-phase differ from the previously reported ones in the literature for the γ-phase.[10,29,30] Particularly, we observe that the ratio of the lattice parameters of the unit cells vary

between the four studies. We estimate that our sample has the largest ratio in *a / b* and the smallest in *c / (a+b)* in comparison with the values reported in literature including $CsPbI_3$ nanocrystals (see ***Table S1)***. The variations on the unit cell parameters might affect the phase stability and the octahedral distortion, therefore also affecting the optoelectronic properties of the material. Such differences in the lattice parameters might be caused by different synthesis methods, composition and different thermal history of the sample and further studies are required to fully understand their correlation. Importantly, our work demonstrates for the first time that pure $CsPbI_3$ can be directly synthesized in a perovskite phase at low temperatures < 60 °C without the need of a post-deposition annealing treatment which is in contrast to many previous reports.[3,17,31] It is important to note that despite the non-stoichiometric composition in most parts of the sample, the XRD linescan shown in ***Figure 1d*** does not indicate the presence of secondary phases, e.g. CsI, PbI_2 or Cs_2PbI_4 for the compositional regime $0.96 \pm 0.1 < [CsI]/[PbI_2]$ 1.07 ± 0.1. However, secondary phases are observed for larger stoichiometric deviations, resulting in CsI segregation for $[CsI]/[PbI_2] > 1.07 \pm 0.1$ and PbI_2 segregation for e $[CsI]/[PbI_2] < 0.96 \pm 0.1$ (see supplementary material ***Figures S2*** and ***S3***) .

To confirm that the position of the phase boundary is directly related to the chemical composition of $[CsI]/[PbI_2] = 1$ and not due to other specific experimental conditions, three combinatorial samples were prepared for which the ratio of the evaporation rate of CsI and PbI_2 was varied, which should lead to a spatial shift of the phase boundary. For each sample, the yellow to brown phase boundary was found at a different sample position. However, the composition at the phase boundary was identical (see ***Figure S4Error! Reference source not found.***). This corroborates that using low temperature processing the brown phase can only be obtained for $[CsI]/[PbI_2] \geq 1$. Because of the significant non-stoichiometry of the γ-$CsPbI_3$ and lack of secondary phases obtained in this study we conclude the presence of a Schottky-defect pair type perovskite structure, which can be described by the chemical formula $Cs_{1+x}Pb_{1-x}I_{3-x}$. The formation of Schottky defect pairs such as [V_{Pb}^{-2} and $2V_I^{+1}$] has been theoretically predicted to have a low formation energy and thus to be thermodynamically favored.[32] Experimentally this has been shown in hybrid perovskites with the incorporation of di-cationic molecules increasing the stability of the phase in so called "hollow" perovskites.[33] The term "hollow" perovskite arises from the abundance of lead and iodine vacancies in the [PbI_3] framework.[33] Starting from $CsPbI_3$, the concentration of these Schottky-defects is expected to increase as x increases and the $Cs_{1+x}Pb_{1-x}I_{3-x}$ phase becomes more CsI rich, which might increase the stability of the perovskite phase in a similar way to what it has been observed in hybrid-hollow perovskites.[33] Alternatively it has been proposed that the stabilization of γ–$CsPbI_3$ is favored

over δ–$CsPbI_3$ by a decreasing grain sizes (or enlarged grain boundary surface area), due to the lower surface energy of the former, compared to the latter phase.[34] In a recent study γ–$CsPbI_3$ has been synthesized by annealing at 100 °C for average grain sizes between 100 nm and 200 nm, where the small grain sizes were obtained by using addition of HI and H2O in the solution process.[34] In the current work small grain sizes between 100 nm and 200 nm are obtained without any additives in the CsI rich region during the evaporation process. On the other hand, somewhat larger grain sizes are observed for the region of the sample crystallizing in the δ–$CsPbI_3$ phase. This could also explain the stabilization of the γ–phase caused be an inhibition of grain growth for samples grown under CsI-excess in the hollow-perovskite region.

Dependence of the optoelectronic properties on composition. The $CsPbI_3$ γ-brown phase shows a sharp absorption onset at about 1.76 eV with absorption coefficient values exceeding $3x10^4$ cm^{-1} as shown for [CsI]/[PbI_2] ≈ 1.10 in ***Figure 2a*** together with a photoluminescence (PL) spectrum acquired under one sun equivalent conditions (see also ***Figure S5)***. It can be seen that the emission is centered at the energy of the absorption onset, indicating that the observed emission band originates from a band-band transition. To investigate the change of the optical properties as a function of CsI/PbI_2 ratio, the PL peak position is plotted as a function of composition in the top graph of ***Figure 2d***. A small blue-shift of the energy of the PL band (PL_{max}) is observed with increasing the CsI/PbI_2 ratio in the brown phase. A similar trend is observed in the external PL quantum yield (EQE_{PL}), which increases from $3x10^{-4}$ % for [CsI]/[PbI_2] ≈ 1.0 to $1x10^{-2}$ % for [CsI]/[PbI_2] ≈ 1.10 indicating that non-radiative recombination is significantly reduced as the $CsPbI_3$ phase becomes more CsI-rich. This is further confirmed by a similar trend observed in the minority carrier lifetime (τ_{SRH}) derived from the TRPL decays shown in ***Figure 2b***, which shows low values τ_{SRH} < 10 ns close to the phase boundary and increases up to a maximum values close to 80 ns [CsI]/[PbI_2] ≈ 1.05. Interestingly, both the EQE_{PL} and the carrier lifetime τ_{SRH} start to decrease again, when the [CsI]/[PbI_2] ratio is increased beyond about 1.05 which is also close to composition when a CsI-segregation becomes detectable. Optical Pump THz Probe (OPTP) measurements allow to characterize the charge carrier dynamics with high temporal resolution,[35] in particular the identification of fast carrier trapping processes in the photoconductivity decays, and the estimation of intra-grain carrier mobilities form their complex frequency response.[36] An overview of such measurements for the sample consisting of the yellow and the brown phase is shown in Figure 2c, where the photoconductivity decay is plotted as a function of the sample position. It can be seen that for the yellow region no photoconductivity response is recorded,

although the samples where excited with fs-pulses above the band gap of the yellow phase. On the other hand in the γ–$CsPbI_3$ region, decay times compatible with the TRPL decays are detected, although decreasing strongly close to the phase boundary (see also SI). Interestingly, the transients do not exhibit any fast decay component within the first picoseconds, which indicates that charge carrier trapping plays a minor role in the recombination kinetics here.

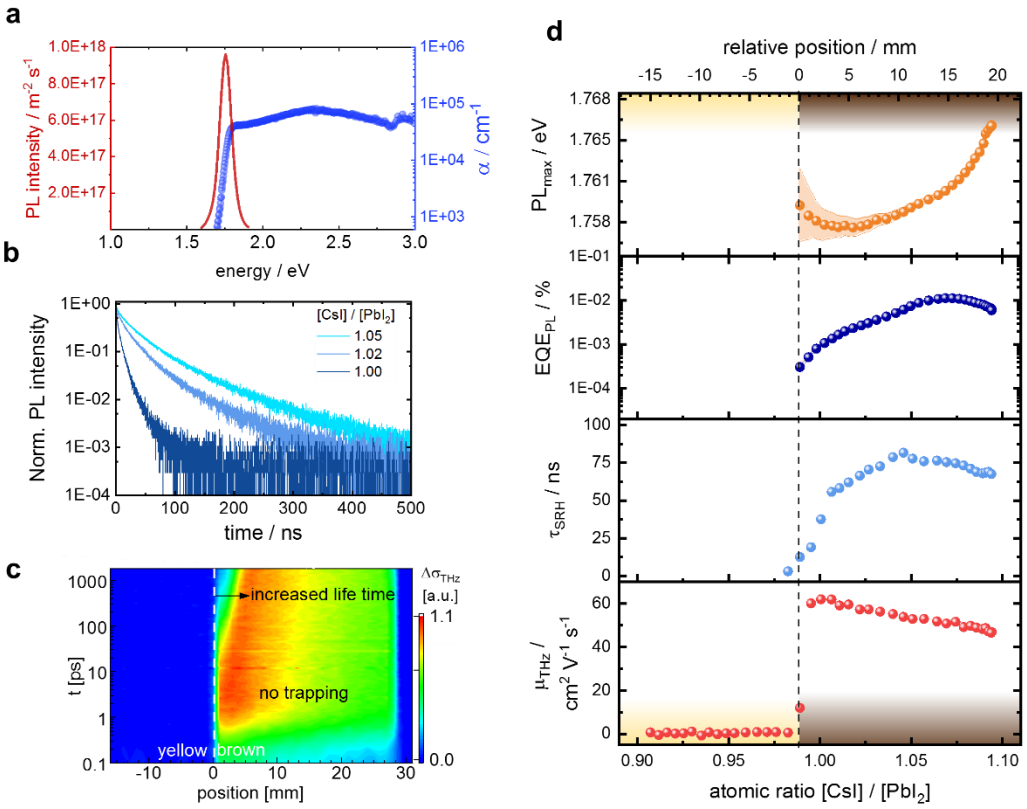

Figure 2 (a) *Absolute intensity PL spectrum and absorption coefficient for [CsI]/[PbI_2] ≈ 1.10 ,* ***(b)*** *TRPL decays as a function of [CsI]/[PbI_2] ratio* ***(c)*** *THz photoconductivity transient map collected at different positions of the sample with different [CsI]/[PbI_2] ratios.* ***(d)*** *Optoelectronic properties determined from the aforementioned measurements as a function of [CsI]/[PbI_2] atomic ratio and relative position on the sample. From top to bottom: Photon energy of the PL maximum (PL_{max}) and external PL quantum yield (EQE_{PL}) extracted from the hyperspectral PL imaging data, minority carrier lifetime (τ_{SRH}) deduced from TRPL and sum mobility (μ_{THz}) deduced from terahertz spectroscopy.*

The sum of electron and hole mobility, μ_{THz}, extracted from the spectral response of the OPTP measurements are shown in ***Figure 2d*** as a function of the composition on the sample. It can be seen that for the yellow δ-phase, the μ_{THz} values are < 0.1 $cm^2V^{-1}s^{-1}$ proving the unsuitability of the yellow phase as a photovoltaic material. On the other hand, large carrier mobilities > 65 $cm^2V^{-1}s^{-1}$ are observed for the brown region (γ-phase) of the sample, which continuously decrease to about 45 $cm^2V^{-1}s^{-1}$ for increasing [CsI]/[PbI_2]. We note that the mobilities observed

for the γ-phase in the present study are similar or higher than the values previously reported for solution processed $CsPbI_3$ films with a post annealing treatment and for $CH_3NH_3PbI_3$ (MAPI).[17,37,38]

Interestingly, opposite to the trend in the carrier lifetime and EQE_{PL}, the carrier mobilities almost immediately decrease as the sample becomes more CsI-rich (see ***Figure S6***). However, this observation may be a direct evidence for the presence of the hollow perovskite structure, which exhibits a decreasing connectivity of its $[PbI_6]$ octahedra building blocks with increasing CsI-content. Whereas in stoichiometric $CsPbI_3$ in the α, β and γ phase,[10] each of the $[PbI_6]$ octahedra share their corners with another octahedron leading to extended wavefunctions of the valence band (halogen *p* orbitals and Pb-*s*-orbitals) and the conduction band (unoccupied Pb-*p* orbitals) this octahedra interconnectivity becomes disrupted for CsI-excess in the so-called hollow perovskites.[39] Thus for increasing CsI-content a reduction in the carrier mobilities is predicted from theory[40] and indeed observed in our experiments. In the δ-phase the $[PbI_6]$ octahedra are present in a non-corner-sharing double-chain, resulting in lower crystallographic dimensionality as well as a less dispersive and thus higher effective mass CBM and VBM[39,40] (see ***Figure 1f***). These properties predict very poor charge carrier mobilities, which again are confirmed in our experiments. The low values of μ_{THz}, the bandgap value of 2.8 eV,[41] and lack of measurable carrier lifetime for this non-perovskite phase, show that this polymorph is not suitable for photovoltaic applications as described by previous reports.[42]

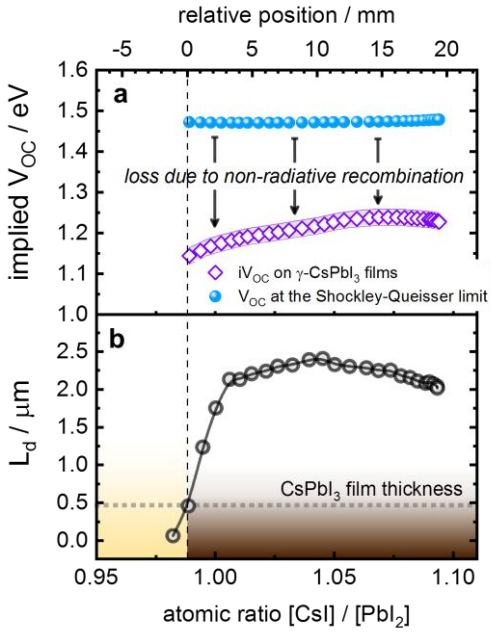

Figure 3 (a) *Implied V_{oc} calculated from absolute PL imaging as a function atomic ratio [CsI]/[PbI_2]. The Shockley-Queisser limit calculated for each position is also shown as a*

reference. ***(b)*** *Diffusion length (L_d) as a fucntion of atomic ratio [CsI]/[PbI_2]. The dotted grey line shows the thickness of the $CsPbI_3$ film.*

The optoelectronic properties reported in the previous section can be combined to assess the charge carrier transport and recombination parameters which are directly relevant to the performance and operation of solar cells based on the investigated materials. To estimate the implied open-circuit voltage (iV_{oc}) of the γ-phase, we calculated the quasi-Fermi level splitting (QFLS) from the photoluminescence data at 300 K as a function of position on the sample (***Figure 3a***). The values were obtained from the calibrated PL spectra at each position in a similar way as reported for mixed cation, mixed halide organic-inorganic perovskites.[43,44] QFLS values between 1.14 and 1.24 ±0.02 eV are obtained, corresponding to the maximum achievable V_{OC} that a given absorber layer could generate in a solar cell, assuming that the charge transport and contact layers do not alter the recombination at the perovskite surface. Figure 3a shows both the QFLS values in the radiative Shockley Queisser limit and the QFLS measured on the $CsPbI_3$ films (iV_{oc}), where the distance between both values indicates the non-radiative recombination losses in the material. It can be seen that as the [CsI]/[PbI_2] ratio increases the non-radiative recombination losses are reduced and the iV_{oc} values become larger. These iV_{oc} values correspond to an EQE_{PL} of approximately ~0.01 % (***Figure 2d***), which is around two orders of magnitude below the EQE_{PL} for bare mixed cation, mixed halide organic-inorganic perovskite films, and similar to the EQE_{PL} measured in ~20 % efficient full stack solar cells.[43,45] This indicates that non-radiative recombination in these inorganic perovskites is still larger than in the mixed cation, mixed halide organic-inorganic perovskites absorber layers used to fabricate high efficiency solar cell devices. With the knowledge of the charge carrier mobilities and lifetimes the diffusion length $L_d = \sqrt{\tau_{SRH}\ \mu\ k_B T/q}$ can be estimated for the investigated films assuming balanced electron and hole mobilities μ_n=μ_p for the sum mobilities derived from OPTP, as the effective masses of electrons and holes are very similar.[46] As can be seen in ***Figure 3b***, the diffusion length is found to be larger than 2 μm for most of the compositional region of the brown phase, except close to the phase boundary, where rapidly decreasing values are derived. We note that the maximum diffusion length observed is about four times larger than the thickness of the film (~450 nm) (see ***Figure 3b***), which clearly shows that the CsI-rich γ-phase investigated in this study is well suited for the fabrication of solar cells.

Photovoltaic performance. P-i-n type (so called "inverted") solar cells were made employing poly(triarylamine) (PTAA) as a hole transporting material and fullerene C_{60} as electron transport layer (***Figure 4a***). The current density - voltage (JV) scan of the best performing device is shown in ***Figure 4b***. Here we achieve a V_{OC} of 0.96 V, a short-circuit current density (J_{SC}) of 17.8 mA/cm^2, a fill factor (FF) of 73 % and a power conversion efficiency (PCE) of above 12 % in the reverse scan. We note that no significant differences are observed in the JV scans as function of scan speed or light soaking (see ***Figure S7***) The stabilized efficiency measured over three minutes by maximum power point (mpp) tracking shows a sharp drop within the first seconds before the PCE settles at 10.7 % (see **Figure 4*c***). It is worth noting that the stabilized PCE is improved to 11.3 % within the first days after preparation and maintains this performance for several weeks which corresponds to a shelf life stability of over 1200 h (see inset in ***Figure 4c***). The current density measured in the JV scan matches quite well with the integrated current density from external quantum efficiency (EQE) of 17.3 mA/cm^2 shown in ***Figure 4d***. The cell shows an EQE of over 80 % over a wide range of the visible spectrum as a consequence of the large L_d values estimated from the TRPL and OPTP data. The drastic loss in measured V_{OC} in the JV scan compared to the iV_{oc} (QFLS) measured on the bare $CsPbI_3$ absorbers, as well as the strong hysteresis, may indicate a misaligned band structure due to non-optimal contact layers or severe interface recombination limiting the device performance. Therefore, optimizing the contact layers is the most promising approach to further increase the efficiency of the presented $CsPbI_3$ solar cell.

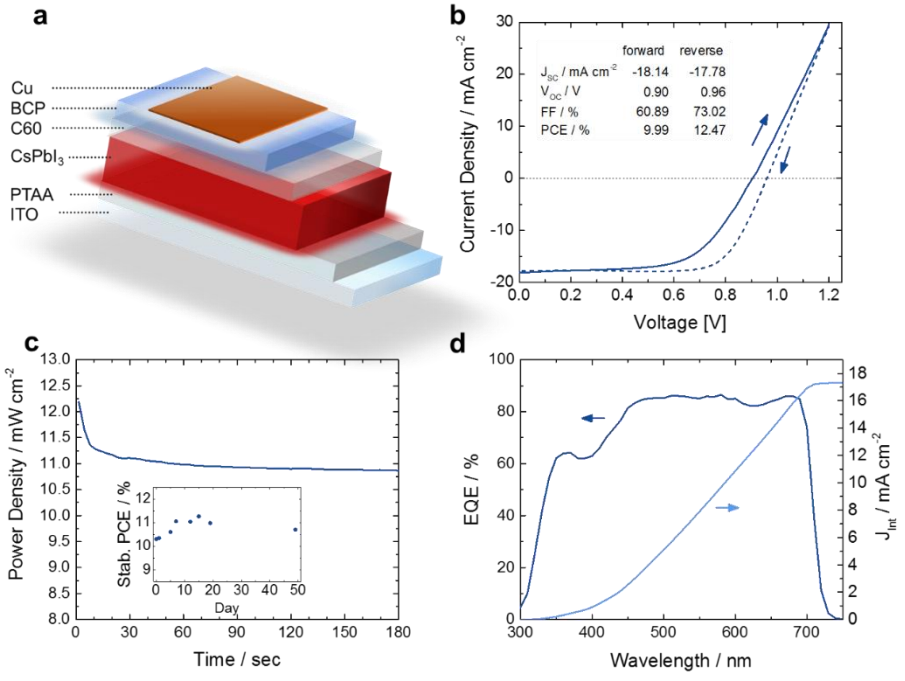

Figure 4 (a) *Schematic of the p-i-n type device configuration used in this work.* ***(b)*** *JV scan of the best performing device measured at day 15 after preparation with a scan rate of 250 mV/s. A strong hysteresis effect between forward and reverse scan is observed as indicated.* ***(c)*** *Power conversion efficiency of the same device over time by maximum power point tracking over 3 minutes. The inset shows the stabilized power conversion efficiency after 3 minutes maximum power point tracking over the course of several weeks.* ***(d)*** *External quantum efficiency (EQE) spectra under 1 sun AM1.5G illumination on the left axis. Integrated photocurrent density from EQE spectra on the right axis.*

In conclusion we have shown that inorganic $CsPbI_3$ can be directly synthesized in the perovskite γ–phase at low temperature by co-evaporation under CsI-rich composition. Direct correspondence between the different polymorphs and their compositional region of stability is obtained employing samples which exhibit a linear gradient in the [CsI]/[PbI_2] ratio. Lack of secondary phases in the CsI-rich regime indicates the presence of a hollow perovskite structure with Schottky defect pairs. Optoelectronic analysis shows promising charge transport and recombination properties with electron and hole sum mobilities above 60 cm^2/Vs and carrier lifetimes larger 70 ns, resulting in large diffusion lengths > 2 μm and an implied V_{oc} of up to 1.24 eV. P-i-n type solar cells fabricated with the γ-$CsPbI_3$ phase obtained by co-evaporation show stabilized efficiencies over 11 % and very high shelf stability of over 1200 h. Since the V_{OC} values of these solar cells are currently about 300 mV smaller than the implied V_{oc} measured for the bare absorber material significant further improvements are expected from a further optimization/exploration of the charge transport and contact layers in these solar cells.

Acknowledgements.

The spatially resolved X-ray diffraction experiments were performed at Beamline BL10 at the DELTA Synchrotron Radiation Facility, Dortmund, Germany. We gratefully acknowledge Dirk Lützenkirchen-Hecht and Ralph Wagner for technical advice and consultation with data analysis as well as the DELTA machine group for providing synchrotron radiation reliably.

The authors acknowledge financial support from the HyPerCells joint Graduate School (www.perovskites.de). A.A.A., M.J. and S.A. are funded by the German Federal Ministry of Education and Research (BMBF), within the project "Materialforschung für die Energiewende" (grant no. 03SF0540). S.A. further acknowledges funding by the German Federal Ministry for Economic Affairs and Energy (BMWi) through the "PersiST" project (grant no. 0324037C).

Additional information

Supplementary information is available in the online version of the paper.

Competing financial interests. The authors declare no competing financial interests.

References

(1) Jeon, N. J.; Na, H.; Jung, E. H.; Yang, T. Y.; Lee, Y. G.; Kim, G.; Shin, H. W.; Il Seok, S.; Lee, J.; Seo, J. A Fluorene-Terminated Hole-Transporting Material for Highly Efficient and Stable Perovskite Solar Cells. *Nat. Energy* **2018**, *3* (8), 1–8. https://doi.org/10.1038/s41560-018-0200-6.

(2) Green, M. A.; Hishikawa, Y.; Dunlop, E. D.; Levi, D. H.; Hohl-Ebinger, J.; Ho-Baillie, A. W. Y. Solar Cell Efficiency Tables (Version 51). *Prog. Photovoltaics Res. Appl.* **2018**, *26* (1), 3–12. https://doi.org/10.1002/pip.2978.

(3) Eperon, G. E.; Paternò, G. M.; Sutton, R. J.; Zampetti, A.; Haghighirad, A. A.; Cacialli, F.; Snaith, H. J. Inorganic Caesium Lead Iodide Perovskite Solar Cells. *J. Mater. Chem. A* **2015**, *3* (39), 19688–19695. https://doi.org/10.1039/c5ta06398a.

(4) Kulbak, M.; Gupta, S.; Kedem, N.; Levine, I.; Bendikov, T.; Hodes, G.; Cahen, D. Cesium Enhances Long-Term Stability of Lead Bromide Perovskite-Based Solar Cells. *J. Phys. Chem. Lett.* **2016**, *7* (1), 167–172. https://doi.org/10.1021/acs.jpclett.5b02597.

(5) Kulbak, M.; Cahen, D.; Hodes, G. How Important Is the Organic Part of Lead Halide Perovskite Photovoltaic Cells? Efficient CsPbBr3 Cells. *J. Phys. Chem. Lett.* **2015**, *6* (13), 2452–2456. https://doi.org/10.1021/acs.jpclett.5b00968.

(6) Stoumpos, C. C.; Malliakas, C. D.; Peters, J. A.; Liu, Z.; Sebastian, M.; Im, J.; Chasapis, T. C.; Wibowo, A. C.; Chung, D. Y.; Freeman, A. J.; et al. Crystal Growth of the Perovskite Semiconductor CsPbBr3: A New Material for High-Energy Radiation Detection. *Cryst. Growth Des.* **2013**, *13* (7), 2722–2727. https://doi.org/10.1021/cg400645t.

(7) Ahmad, W.; Khan, J.; Niu, G.; Tang, J. Inorganic $CsPbI_3$ Perovskite-Based Solar Cells: A Choice for a Tandem Device. *Sol. RRL* **2017**, *1* (7), 1700048. https://doi.org/10.1002/solr.201700048.

(8) Wang, P.; Zhang, X.; Zhou, Y.; Jiang, Q.; Ye, Q.; Chu, Z.; Li, X.; Yang, X.; Yin, Z.; You, J. Solvent-Controlled Growth of Inorganic Perovskite Films in Dry Environment for Efficient and Stable Solar Cells. *Nat. Commun.* **2018**, *9* (1), 2225. https://doi.org/10.1038/s41467-018-04636-4.

(9) Sanehira, E. M.; Marshall, A. R.; Christians, J. A.; Harvey, S. P.; Ciesielski, P. N.; Wheeler, L. M.; Schulz, P.; Lin, L. Y.; Beard, M. C.; Luther, J. M. Enhanced Mobility CsPbI3quantum Dot Arrays for Record-Efficiency, High-Voltage Photovoltaic Cells. *Sci. Adv.* **2017**, *3* (10),

eaao4204. https://doi.org/10.1126/sciadv.aao4204.

(10) Marronnier, A.; Roma, G.; Boyer-Richard, S.; Pedesseau, L.; Jancu, J. M.; Bonnassieux, Y.; Katan, C.; Stoumpos, C. C.; Kanatzidis, M. G.; Even, J. Anharmonicity and Disorder in the Black Phases of Cesium Lead Iodide Used for Stable Inorganic Perovskite Solar Cells. *ACS Nano* **2018**, *12* (4), 3477–3486. https://doi.org/10.1021/acsnano.8b00267.

(11) Stoumpos, C. C.; Malliakas, C. D.; Kanatzidis, M. G. Semiconducting Tin and Lead Iodide Perovskites with Organic Cations: Phase Transitions, High Mobilities, and near-Infrared Photoluminescent Properties. *Inorg. Chem.* **2013**, *52* (15), 9019–9038. https://doi.org/10.1021/ic401215x.

(12) Hu, Y.; Bai, F.; Liu, X.; Ji, Q.; Miao, X.; Qiu, T.; Zhang, S. Bismuth Incorporation Stabilized α-CsPbI3for Fully Inorganic Perovskite Solar Cells. *ACS Energy Lett.* **2017**, *2* (10), 2219–2227. https://doi.org/10.1021/acsenergylett.7b00508.

(13) Swarnkar, A.; Marshall, A. R.; Sanehira, E. M.; Chernomordik, B. D.; Moore, D. T.; Christians, J. A.; Chakrabarti, T.; Luther, J. M. Quantum Dot-Induced Phase Stabilization of -CsPbI3 Perovskite for High-Efficiency Photovoltaics. *Science (80-.).* **2016**, *354* (6308), 92–95. https://doi.org/10.1126/science.aag2700.

(14) Sutton, R. J.; Eperon, G. E.; Miranda, L.; Parrott, E. S.; Kamino, B. A.; Patel, J. B.; Hörantner, M. T.; Johnston, M. B.; Haghighirad, A. A.; Moore, D. T.; et al. Bandgap-Tunable Cesium Lead Halide Perovskites with High Thermal Stability for Efficient Solar Cells. *Adv. Energy Mater.* **2016**, *6* (8), n/a-n/a. https://doi.org/10.1002/aenm.201502458.

(15) Pistor, P.; Burwig, T.; Fra, W. Crystal Phases and Thermal Stability of Co-Evaporated CsPbX 3 (X = I, Br) Thin Films¨. **2018**, *3*. https://doi.org/10.1021/acs.jpclett.8b02059.

(16) Frolova, L. A.; Anokhin, D. V.; Piryazev, A. A.; Luchkin, S. Y.; Dremova, N. N.; Stevenson, K. J.; Troshin, P. A. Highly Efficient All-Inorganic Planar Heterojunction Perovskite Solar Cells Produced by Thermal Coevaporation of CsI and PbI2. *J. Phys. Chem. Lett.* **2017**, *8* (1), 67–72. https://doi.org/10.1021/acs.jpclett.6b02594.

(17) Vapour-Deposited Cesium Lead Iodide Perovskites: Microsecond Charge Carrier Lifetimes and Enhanced Photovoltaic Performance. *ACS Energy Lett.* **2017**, *2* (8), 1901–1908. https://doi.org/10.1021/acsenergylett.7b00591.

(18) Chen, C. Y.; Lin, H. Y.; Chiang, K. M.; Tsai, W. L.; Huang, Y. C.; Tsao, C. S.; Lin, H. W. All-Vacuum-Deposited Stoichiometrically Balanced Inorganic Cesium Lead Halide Perovskite Solar Cells with Stabilized Efficiency Exceeding 11%. *Adv. Mater.* **2017**, *29* (12), 1605290. https://doi.org/10.1002/adma.201605290.

(19) Ma, Q.; Huang, S.; Chen, S.; Zhang, M.; Lau, C. F. J.; Lockrey, M. N.; Mulmudi, H. K.; Shan, Y.; Yao, J.; Zheng, J.; et al. The Effect of Stoichiometry on the Stability of Inorganic Cesium Lead Mixed-Halide Perovskites Solar Cells. *J. Phys. Chem. C* **2017**, *121* (36), 19642–19649. https://doi.org/10.1021/acs.jpcc.7b06268.

(20) Ma, Q.; Huang, S.; Wen, X.; Green, M. A.; Ho-Baillie, A. W. Y. Hole Transport Layer Free Inorganic CsPbIBr2 Perovskite Solar Cell by Dual Source Thermal Evaporation. *Adv. Energy Mater.* **2016**, *6* (7), n/a-n/a. https://doi.org/10.1002/aenm.201502202.

(21) Chen, H.; Xiang, S.; Li, W.; Liu, H.; Zhu, L.; Yang, S. Inorganic Perovskite Solar Cells: A Rapidly Growing Field. *Sol. RRL* **2018**, *2* (2), 1700188. https://doi.org/10.1002/solr.201700188.

(22) Beal, R. E.; Slotcavage, D. J.; Leijtens, T.; Bowring, A. R.; Belisle, R. A.; Nguyen, W. H.; Burkhard, G. F.; Hoke, E. T.; McGehee, M. D. Cesium Lead Halide Perovskites with Improved Stability for Tandem Solar Cells. *J. Phys. Chem. Lett.* **2016**, *7* (5), 746–751. https://doi.org/10.1021/acs.jpclett.6b00002.

(23) Lau, C. F. J.; Zhang, M.; Deng, X.; Zheng, J.; Bing, J.; Ma, Q.; Kim, J.; Hu, L.; Green, M. A.; Huang, S.; et al. Strontium-Doped Low-Temperature-Processed CsPbI2Br Perovskite Solar Cells. *ACS Energy Lett.* **2017**, *2* (10), 2319–2325. https://doi.org/10.1021/acsenergylett.7b00751.

(24) Wang, Q.; Zheng, X.; Deng, Y.; Zhao, J.; Chen, Z.; Huang, J. Stabilizing the α-Phase of CsPbI3Perovskite by Sulfobetaine Zwitterions in One-Step Spin-Coating Films. *Joule* **2017**, *1* (2), 371–382. https://doi.org/10.1016/j.joule.2017.07.017.

(25) Eperon, G. E.; Paternò, G. M.; Sutton, R. J.; Zampetti, A.; Haghighirad, A. A.; Cacialli, F.; Snaith, H. J. Inorganic Caesium Lead Iodide Perovskite Solar Cells. *J. Mater. Chem. A* **2015**, *3* (39), 19688–19695. https://doi.org/10.1039/c5ta06398a.

(26) Zhang, T.; Dar, M. I.; Li, G.; Xu, F.; Guo, N.; Grätzel, M.; Zhao, Y. Bication Lead Iodide 2D Perovskite Component to Stabilize Inorganic A-CsPbI3perovskite Phase for High-Efficiency Solar Cells. *Sci. Adv.* **2017**, *3* (9), e1700841. https://doi.org/10.1126/sciadv.1700841.

(27) Li, F.; Pei, Y.; Xiao, F.; Zeng, T.; Yang, Z.; Xu, J.; Sun, J.; Peng, B.; Liu, M. Tailored Dimensionality to Regulate the Phase Stability of Inorganic Cesium Lead Iodide Perovskites. *Nanoscale* **2018**, *10* (14), 6318–6322. https://doi.org/10.1039/c8nr00758f.

(28) Jiang, Y.; Yuan, J.; Ni, Y.; Yang, J.; Wang, Y.; Jiu, T.; Yuan, M.; Chen, J. Reduced-Dimensional α-CsPbX3Perovskites for Efficient and Stable Photovoltaics. *Joule* **2018**. https://doi.org/10.1016/j.joule.2018.05.004.

(29) Coherent Nanotwins and Dynamic Disorder in Cesium Lead Halide Perovskite Nanocrystals. *ACS Nano* **2017**, *11* (4), 3819–3831. https://doi.org/10.1021/acsnano.7b00017.

(30) Sutton, R. J.; Filip, M. R.; Haghighirad, A. A.; Sakai, N.; Wenger, B.; Giustino, F.; Snaith, H. J. Cubic or Orthorhombic? Revealing the Crystal Structure of Metastable Black-Phase CsPbI 3 by Theory and Experiment. *ACS Energy Lett.* **2018**, *3* (8), 1787–1794. https://doi.org/10.1021/acsenergylett.8b00672.

(31) Dastidar, S.; Hawley, C. J.; Dillon, A. D.; Gutierrez-Perez, A. D.; Spanier, J. E.; Fafarman, A. T. Quantitative Phase-Change Thermodynamics and Metastability of Perovskite-Phase Cesium Lead Iodide. *J. Phys. Chem. Lett.* **2017**, *8* (6), 1278–1282.

https://doi.org/10.1021/acs.jpclett.7b00134.

(32) Walsh, A.; Scanlon, D. O.; Chen, S.; Gong, X. G.; Wei, S. H. Self-Regulation Mechanism for Charged Point Defects in Hybrid Halide Perovskites. *Angew. Chemie - Int. Ed.* **2015**, *54* (6), 1791–1794. https://doi.org/10.1002/anie.201409740.

(33) Spanopoulos, I.; Ke, W.; Stoumpos, C. C.; Schueller, E. C.; Kontsevoi, O. Y.; Seshadri, R.; Kanatzidis, M. G. Unraveling the Chemical Nature of the 3D " Hollow " Hybrid Halide Perovskites. **2018**. https://doi.org/10.1021/jacs.8b01034.

(34) Zhao, B.; Jin, S.-F.; Huang, S.; Liu, N.; Ma, J.-Y.; Xue, D.-J.; Han, Q.; Ding, J.; Ge, Q.-Q.; Feng, Y.; et al. Thermodynamically Stable Orthorhombic γ-CsPbI 3 Thin Films for High-Performance Photovoltaics. *J. Am. Chem. Soc.* **2018**, *140* (37), 11716–11725. https://doi.org/10.1021/jacs.8b06050.

(35) Jepsen, P. U.; Cooke, D. G.; Koch, M. Terahertz Spectroscopy and Imaging - Modern Techniques and Applications. *Laser Photon. Rev.* **2011**, *5* (1), 124–166. https://doi.org/10.1002/lpor.201000011.

(36) Hempel, H.; Redinger, A.; Repins, I.; Moisan, C.; Larramona, G.; Dennler, G.; Handwerg, M.; Fischer, S. F.; Eichberger, R.; Unold, T. Intragrain Charge Transport in Kesterite Thin Films - Limits Arising from Carrier Localization. *J. Appl. Phys.* **2016**, *120* (17). https://doi.org/10.1063/1.4965868.

(37) Dastidar, S.; Li, S.; Smolin, S. Y.; Baxter, J. B.; Fafarman, A. T. Slow Electron-Hole Recombination in Lead Iodide Perovskites Does Not Require a Molecular Dipole. *ACS Energy Lett.* **2017**, *2* (10), 2239–2244. https://doi.org/10.1021/acsenergylett.7b00606.

(38) Staub, F.; Hempel, H.; Hebig, J. C.; Mock, J.; Paetzold, U. W.; Rau, U.; Unold, T.; Kirchartz, T. Beyond Bulk Lifetimes: Insights into Lead Halide Perovskite Films from Time-Resolved Photoluminescence. *Phys. Rev. Appl.* **2016**, *6* (4), 044017. https://doi.org/10.1103/PhysRevApplied.6.044017.

(39) Xiao, Z.; Yan, Y. Progress in Theoretical Study of Metal Halide Perovskite Solar Cell Materials. *Adv. Energy Mater.* **2017**, *7* (22), 1701136. https://doi.org/10.1002/aenm.201701136.

(40) Xiao, Z.; Meng, W.; Wang, J.; Mitzi, D. B.; Yan, Y. Searching for Promising New Perovskite-Based Photovoltaic Absorbers: The Importance of Electronic Dimensionality. *Mater. Horizons* **2017**, *4* (2), 206–216. https://doi.org/10.1039/c6mh00519e.

(41) Kim, Y. G.; Kim, T.-Y.; Oh, J. H.; Choi, K. S.; Kim, Y.-J.; Kim, S. Y. Cesium Lead Iodide Solar Cells Controlled by Annealing Temperature. *Phys. Chem. Chem. Phys.* **2017**, *19* (8), 6257–6263. https://doi.org/10.1039/C6CP08177K.

(42) Ripolles, T. S.; Nishinaka, K.; Ogomi, Y.; Miyata, Y.; Hayase, S. Efficiency Enhancement by Changing Perovskite Crystal Phase and Adding a Charge Extraction Interlayer in Organic Amine Free-Perovskite Solar Cells Based on Cesium. *Sol. Energy Mater. Sol. Cells* **2016**, *144*, 532–536. https://doi.org/10.1016/j.solmat.2015.09.041.

(43) Stolterfoht, M.; Wolff, C. M.; Márquez, J. A.; Zhang, S.; Hages, C. J.; Rothhardt, D.; Albrecht, S.; Burn, P. L.; Meredith, P.; Unold, T.; et al. Visualization and Suppression of Interfacial Recombination for High-Efficiency Large-Area Pin Perovskite Solar Cells. *Nat. Energy* **2018**. https://doi.org/10.1038/s41560-018-0219-8.

(44) Ross, R. T. Some Thermodynamics of Photochemical Systems. *J. Chem. Phys.* **1967**, *46* (12), 4590–4593. https://doi.org/10.1063/1.1840606.

(45) Liu, Z.; Krückemeier, L.; Krogmeier, B.; Klingebiel, B.; Márquez, J. A.; Levcenko, S.; Öz, S.; Mathur, S.; Rau, U.; Unold, T.; et al. Open-Circuit Voltages Exceeding 1.26 V in Planar Methylammonium Lead Iodide Perovskite Solar Cells. *ACS Energy Lett.* **2018**, 110–117. https://doi.org/10.1021/acsenergylett.8b01906.

(46) Afsari, M.; Boochani, A.; Hantezadeh, M. Electronic, Optical and Elastic Properties of Cubic Perovskite CsPbI3: Using First Principles Study. *Optik (Stuttg).* **2016**, *127* (23), 11433–11443. https://doi.org/10.1016/j.ijleo.2016.09.013.